ERT Data Assimilation to Characterize Aquifer Hydraulic Conductivity Heterogeneity through a Heat-tracing Experiment

Benyamin Shariatinik [1], Erwan Gloaguen [1], Jasmin Raymond[1], Louis-Charles Boutin[1], Gabriel Fabien-Ouellet[2]

1. Centre Eau Terre Environnement, Institut National de la Recherche Scientifique (INRS), Québec, QC G1K 9A9, Canada

2. Department of Civil, Geological and Mining Engineering, Polytechnique Montréal, Montréal, QC, H3T 1J4, Canada

Correspondance

Benyamin Shariatinik, Centre Eau Terre Environnement, Institut National de la Recherche Scientifique (INRS), Québec, QC G1K 9A9, Canada.

E-mail : Benyamin.Shariatinik@inrs.ca

Abstract

Geothermal Energy Systems such as heat pump relying on aquifers uses renewable sources of energy that are accessible in urban areas. It is necessary to characterize the subsurface hydraulic properties prior to the installation of such systems. In this context, heat tracing experiment is a typical field test that can help with characterization of the subsurface. During a heat tracing experiment, monitoring with downhole temperature sensors, water-level pressure transducers and electrical resistivity tomography (ERT) can be used to help to characterize the hydrogeological properties. Previous monitoring tools have shortcomings such as low-resolution data and over-smoothing, thus they fail to reproduce the heterogeneity of hydrogeological properties. Ensemble Kalman filter (EnKF) is a promising tool that can overcome the over-smoothing problem to replicate the hydrogeological property heterogeneity. In this work, we proposed a new procedure to assimilate time-lapse cross-borehole ERT data into a numerical model of groundwater flow and heat transfer, where the ground water is extracted, and heated water is reinjected into an unconfined sandy-gravel aquifer. The finite element model (FEFLOW 7.3) of groundwater flow and heat transfer is integrated with petrophysical relationship and electrical forward modeling (Resipy) to estimate cross-borehole ERT measurements. Then, the estimated apparent resistivity is assimilated to update the hydraulic conductivity model using EnKF. The results of the application of the proposed approach to a experimental site located in Quebec City (Canada) demonstrate that the heterogeneity of K is correctly reproduce since the updated K model is reasonably consistent with the lithological log. In addition, the proposed approach was able to replicate the cross-borehole ERT field and temperature measurements. The comparison between prior and posterior distribution of K with slug test results shows that the EnKF made the final (assimilated) distribution of K move toward K values inferred with slug tests.

Data Availability Statement

The data that support the findings of this study are available on the request from corresponding author. The data are not publicly available due to privacy. There is no conflict.

1.Introduction

The recent climate crisis is mostly attributed to fossil fuel consumption (Maslin 2004). Development of renewable sources of energies is important to reduce such fuel consumption. Shallow Geothermal Energy Systems (SGES) relying on groundwater heat pumps and wells installed in aquifers at a depth of less than 200 m and with a temperature lower than 25 °C is now considered a sustainable heating and cooling option (Raymond 2018; Xu et al. 2020). SGES takes advantages of the earth thermal inertia considered a renewable source of energy worthwhile to be developed (Bayer et al. 2019). Indeed, SGES in urban areas is considered as an effective solution to reduce fossil fuel consumption in our path to decarbonization, especially by providing residential and commercial buildings with lower emission heating/cooling technology compared to conventional systems (Raymond 2018). For these goals, characterization of subsurface hydrogeological properties is crucial to develop, exploit, manage and preserve geothermal resources in a sustainable manner (Cultrera et al. 2018). Characterizing the subsurface allows for an optimal design of groundwater heat pump systems, which can lower the costs and facilitate the development of the technology (Hermans et al. 2015).

There are three main types of geothermal heat pumps including groundwater heat pump (open loop), surface water heat pumps (open and closed loop) and ground-coupled heat pump (closed loop). The groundwater heat pump (GWHP) system operates by pumping ground water and reinjecting it back into the aquifer. Thus, the heat transfer in the GWHP system is dominated by advection heat transfer mode (Kaviany 1995). Therefore, it is essential to estimate aquifer hydraulic conductivity heterogeneity prior to the installation of the GWHP system to guarantee the sustainable short/long-term functionality of the system.

In the scope of SGES design, heat-tracing experiments are conducted to characterize the aquifer's hydraulic properties (Saar 2011; Anderson 2005). The experiment can be performed jointly with downhole temperature monitoring and time-lapse electrical resistivity tomography (ERT) as monitoring tools. Although both preceding monitoring tools have been used successfully in several projects, they suffer from some drawbacks. The downhole temperature monitoring captures the local state of the system only; thus, it suffers from limited spatial coverage and resolution. To tackle the data resolution shortcoming, geophysical methods have been proposed. Amongst them, the ERT method is popular for hydrogeological characterization, since time-lapse ERT measurements can capture the dynamic variation in hydrogeological state of the subsurface. The time-lapse ERT method allows a dense spatial coverage of the electrical resistivity in 2D/3D permitting to investigate shallow subsurface dynamic variations in hydrogeological state (Binley et al. 2015). In recent

decades, the time-lapse ERT has been implemented successfully to characterize thermal plume geometries (Aghasi et al. 2013) or imaging the spatial and temporal movement of plume (Pidlisecky et al. 2011; Singha & M. Gorelick 2006). The shortcoming associated with regularized ERT inversion is over smoothing, hence the high values of the inverted parameters are underestimated (Day-Lewis et al. 2005).

The Bayesian assimilation method has been used increasingly in the recent years for hydrogeological applications (Yan & Dongxiao 2006; Tso et al. 2020; Bouzaglou et al. 2018; Camporese et al. 2008). The idea is to integrates time-lapse ERT measurements and numerical models of groundwater flow to better characterize the current state of the system (Wikle & Berliner 2007). The Bayesian assimilation can provide a better prediction of a future state of the system which is the task that monitoring tools fail to accomplish. In (Tso et al. 2020), Ensemble Smoother with Multiple Data Assimilation (ES-MDA) approach has been proposed to identify various leak detection parameters using time-lapse ERT data. As an effort to estimate the soil hydraulic properties in a laboratory experiment of saltwater intrusion, monitored-ERT data were assimilated into a numerical model of groundwater flow and contaminant transport using EnKF (Bouzaglou et al. 2018).

In this study, we proposed a new implementation of time-lapse ERT data assimilation to assess the potential of EnKF (Evensen 1994) to estimate the hydraulic conductivity (K) heterogeneity within an aquifer during a heat-tracing experiment conducted in the scope of GWHP system design. We also want to evaluate the ability of EnKF to tackle the field experimental uncertainties such as measurements uncertainties. To this end, a heat tracing experiment was performed to pump groundwater and reinject heated water into an uncontained sandy-gravel aquifer, the experimental site located in Quebec City, Canada. Groundwater temperatures were monitored at the pumping and injection wells, and surrounding monitoring wells. A time-lapse cross-borehole ERT survey was conducted during the heat-tracing experiment to monitor the subsurface resistivity change. Moreover, A finite element numerical model of groundwater flow and heat transfer (FEFLOW 7.3) (Diersch 2014) was developed to reproduce the heat-tracing experiment. At each ERT monitoring time-step, the simulated subsurface temperature model is converted to electrical conductivity using petrophysical relationship. Then the resulting electrical conductivity model is used to perform an electrical forward modeling with Resipy (Saneiyan et al. 2018). The electrical forward modeling provides the ERT measurements at the same measuring points coordinates as the ERT field measurements. Finally, the ERT field measurements are assimilated into the heat transfer model by means of EnKF approach to update the K model.

The paper is organized as follows: first, we present the new approach for ERT data assimilation, second the study area and field setup are described, then the results of time-lapse cross-borehole ERT data assimilation are presented.

2. Methodology

2.1. Experimental procedure

In this study, a new procedure including the implementation of EnKF to assimilate time-lapse cross-borehole ERT data in a heat tracing experiment is tested, in order to investigate the capability to characterize the heterogeneity of aquifers by means of the hydraulic conductivity. The proposed workflow composed of six major steps that are repeated for each monitoring time step (Figure 1).

In the context of EnKF, the ensemble refers to a set of equiprobable scenarios of desired variable to be updated. The scenarios are generated based on our best prior knowledge of the system. Here, a set of hydraulic conductivity realizations (ensemble) are provided based on the results of the Slug tests, the lithological log and previous works (Hwang et al. 2017) at the beginning of the process. Then, the ensemble is propagated through a transition function (forward transient simulation of groundwater flow and heat transfer) to simulate the subsurface temperature responses to the heat-tracing experiment. The computed temperatures are converted to a 3D electrical resistivity distribution using petrophysical relationship. An electrical forward model using 3D electrical resistivity distribution computed in the last step is performed to predict the subsurface apparent electrical resistivity at the location of electrodes. Finally, the cross-borehole ERT field measurements (observations) and predicted apparent electrical resistivity (output of electrical forward modeling) is assimilated to update the hydraulic conductivity within the ensemble. In the following subsections, each step of the workflow is discussed in detail.
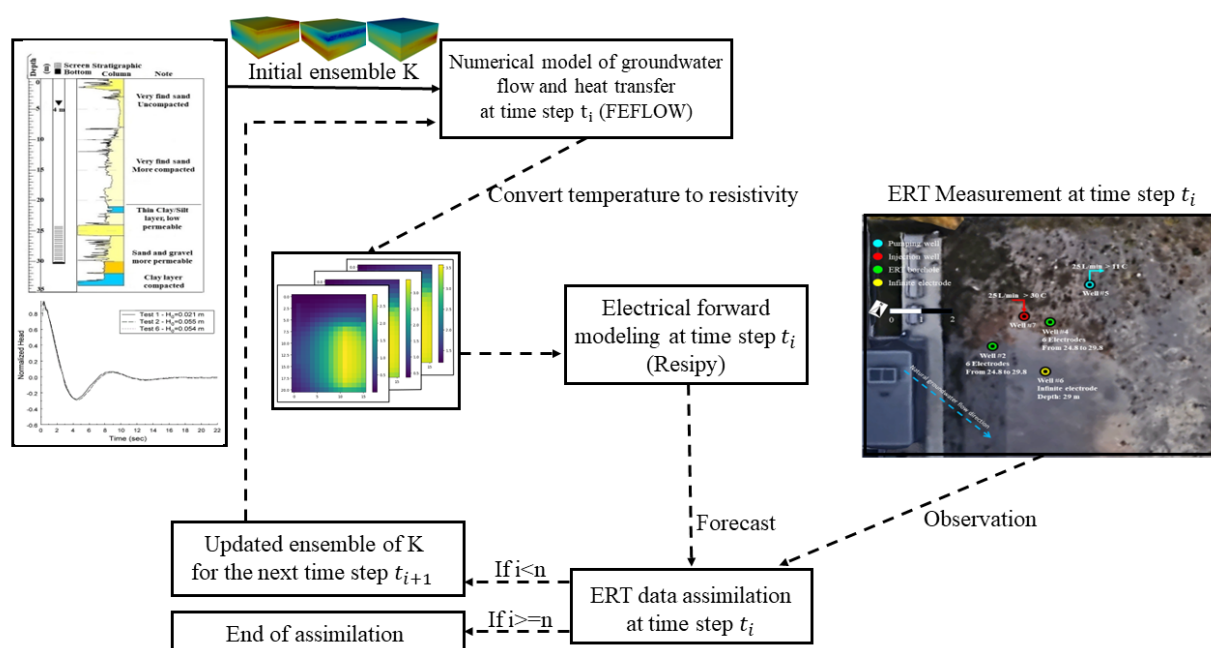

Figure 1 The workflow shows the implementation of time-lapse cross-borehole ERT data assimilation to calibrate subsurface 3D distribution of hydraulic conductivities. n refer to the number of monitoring time-steps.

2.2. Petrophysical relationship and electrical forward modelling

There is a well-known petrophysical relationship (Equation 1) to quantify the link between electrical conductivity and fluid temperature (Hayley et al. 2007; Hermans et al. 2012).

$$\frac{\sigma_{f,T}}{\sigma_{f,10.3}} = m_f(T - 10) + 1 \tag{1}$$

where $\sigma_{f,T}$ refer to water electrical conductivity (S.m^{-1}) at temperature T in ^{o}C and $\sigma_{f,10.3}$ is the water electrical conductivity at baseline temperature 10.3 ^{o}C, m_f is the fractional change in water electrical conductivity per degree Celsius at pore water baseline temperature. According to previous studies we considered the value of m_f equal to 0.0198 (Hayley et al. 2007). (Hermans et al. 2015) Given that our experiment is conducted in a sandy gravel aquifer, the surface electrical conductivity is negligible. Therefore, the measured change in electrical conductivity is assumed to reflect the change in temperature in the subsurface for both the matrix and pore fluid. The relationship between bulk matrix and pore fluid electrical conductivity can be derived using Archie's law (Archie 1942):

$$\sigma_{f,T} = \frac{\sigma_{b,T}}{\sigma_{b,10.3}} \sigma_{f,10.3} \tag{2}$$

Here, $\sigma_{b,T}$ represent bulk electrical conductivity at temperature T and $\sigma_{b,10.3}$ is bulk electrical conductivity at baseline temperature of 10.3 ^{o}C.

We insert Equation 2 into Equation 1 in order to calculate the bulk electrical resistivity by using a given subsurface temperature distribution at each time step t.

$$\sigma_{b,T} = \sigma_{b,10.3}\big((T - 10.3)m_f + 1\big) \tag{3}$$

Here T_t is a 3D matrix representing the temperature at each node for a given time step t, where $\sigma_{b,t}$ represents converted bulk electrical conductivity at the time step t_i.

As the next step of the workflow, the electrical forward modeling is performed using electrical resistivity models to measure the modeled apparent resistivity with same electrode coordinates and array as the field measurements. An essential part of ERT data assimilation scheme is the numerical simulation of measurements for a given model of bulk electrical resistivity at each time step; The electrical forward modeling is carried out using ResIPy, an open-source software that performs electrical forward modeling and inversion (Blanchy 2020).

2.3. Assimilation of ERT data

Data assimilation is an effective approach to combine the numerical model and observations to produce an output model which is more accurate than both the numerical model and observations. Evensen (1994) proposed the EnKF which is Monte Carlo

approximation of the traditional template of KF (Evensen 2009). In this study (Figure 1), the ensemble (**E**) refers to the ensemble of 100 realizations of hydraulic conductivity (K) which is the variable to be updated (Nima Raanes 2016):

$$\mathbf{E} = [\text{realization}_1, \text{realization}_2, \ldots, \text{realization}_{100}] \tag{4}$$

The EnKF consists of the recursion application of two main steps.

1. Forecast:

Considering a transient model of the ground water flow and heat transfer, the ensemble of K is integrated forward in time and the apparent electrical resistivity is modeled at each monitoring time step using the following equations.

$$\mathbf{E}_{t+1}^{T} = F\big(\mathbf{E}_t^{K,a}\big) + \mathbf{q}_t \tag{5}$$

$$\boldsymbol{y}_t = H(\mathbf{E}_t^{R}) + \mathbf{r}_t \tag{6}$$

where $\mathbf{E}_{t+1}^{T}$ is the ensemble of computed subsurface temperature distribution T at the time t+1, F refers to numerical model of the ground water flow and heat transfer, $\mathbf{E}_t^{K,a}$ represent the updated ensemble of K at time t, $\mathbf{q}_t$ is the model error. It should be noticed that $\mathbf{E}_0^{K,a}$ (first time step t=0) is equal to the initial ensemble of K. The function H is the electrical forward modeling function that links K to the modeled apparent electrical resistivity. The $\boldsymbol{y}_t$ is the estimated apparent resistivity at time t which is calculated by propagating converted apparent electrical resistivity ensemble ($\mathbf{E}_t^{R}$) (Equation 3) via the electrical forward modeling function (H) and $\mathbf{r}_t$ refers to the error of measured apparent electrical resistivity.

2. Analysis:

The updated ensemble of K at the preceding monitoring time-step ($\mathbf{E}_{t-1}^{K,a}$) is reinitialized using the following equation:

$$\mathbf{E}_t^{K,a} = \mathbf{E}_{t-1}^{K,a} + \overline{\mathbf{K}}\{\boldsymbol{y}_t + \mathbf{D}_{obs} - H(\mathbf{E}_t^{R})\} \tag{7}$$

where, the $\mathbf{E}_t^{K,a}$ is the updated (posterior) ensemble of K at time step t, $\overline{\mathbf{K}}$ is Kalman Gain (KG), $\mathbf{y}_t$ is the apparent electrical resistivity field measurements at monitoring time step t and $\mathbf{D}_{obs}$ represents observation perturbation that is a sampled independent and identically distributed distribution from error model of apparent electrical resistivity field measurements.

Therefore, the updated ensemble of K at time step t can be seen as a weighted average of $\mathbf{E}_{t-1}^{K,a}$ and measurements. The KG can be expressed as follows:

$$\overline{\mathbf{K}} = \overline{\mathbf{P}}^{\,f}\mathbf{H}^T\big(\mathbf{H}\overline{\mathbf{P}}^{\,f}\mathbf{H}^T + \mathbf{R}\big)^{-1} \qquad (8)$$

where $\overline{\mathbf{P}}^{\,f}$ represents the forecast error covariance matrix of the $\mathbf{E}_{t-1}^{K,a}$, $\mathbf{R}$ is the measurement error covariance matrix. The two preceding matrices assessing the accuracy of the assimilation results are respectively expressed as:

$$\overline{\mathbf{P}}_{i,j}^{f} = \frac{1}{N-1}\big(\mathbf{E}_{i,1:N}^{K,a} - \overline{\mathbf{E}}_i^{K,a}\big)\cdot\big(\mathbf{E}_{j,1:N}^{K,a} - \overline{\mathbf{E}}_j^{K,a}\big)^T \qquad (9)$$

$$\mathbf{R} = \frac{\mathbf{D}_{obs}\mathbf{D}_{obs}{}^T}{N-1} \qquad (10)$$

where, $\overline{\mathbf{E}}_i^{K,a}$ represents the mean value of ith row of $\mathbf{E}_{t-1}^{K,a}$, i and j represent the row and column of ensemble matrix respectively and N is the ensemble size.

The finite ensemble size often leads to spurious correlation over long distances between state variable and observation that results in a spurious update in the state variable during the analysis steps of assimilation experiment (Evensen 2009). The spurious updates can bring about a decrease in ensemble variance. On the other hand, using large ensemble size increase the computational cost dramatically thus one need to trade-off between ensemble size and available computational capability in order to obtain an acceptable running time and ensemble variance reduction. The multiplicative covariance inflation technique is another solution to cancel out the spurious correlation effect where the measurement error covariance model is multiplied by an inflation factor at each assimilation step (Evensen, 2009). In this study we used an inflation factor of 0.01 to compensate the spurious correlation effects.

3. Study area

3.1 Hydrogeological framework

The heat-tracing experiment was conducted at a site in Quebec City, Canada, near the Baie de Beauport, northern shore of the St-Lawrence River (Figure 2). The hydrostratigraphic cross-section of Proto-St-Lawrence's delta situated at the base of Quebec City consisting of the bed rock which is overtopped by the sediments of the upper Wisconsinan to pre-Wisconsinan (Lamarche 2011) consisting mainly of heterogeneous sand or gravel layers. Deep-water marine sediments composed of silt cover this unit. Deltaic sediments of the Proto-St-Lawrence composed of sand and a thin gravel layer at the base cover the previous unit. On the surface, alluvial deposits of estuarine and fluvial origin form a layer of sandy silt (Poulin et al. 2013).

Subsurface site characterization was initiated using cone penetration test (CPT) to further understand lithologies present at the site scale. Figure 3a shows the configuration of

monitoring wells and Figure 3b shows the CPT for Well #2 (b). site: on the CPT results, the lithostratigraphy at the study site is interpreted to be a sequence of five distinct units from the bottom to the top: i) compacted clay; ii) sand and gravel at a depth ranging from 24 m to 30 m below the ground surface which is interpreted to be the main aquifer at the site; iii) a thin clay/silt unit and iv) and v) two units of more compacted and uncompacted very fine sand respectively.
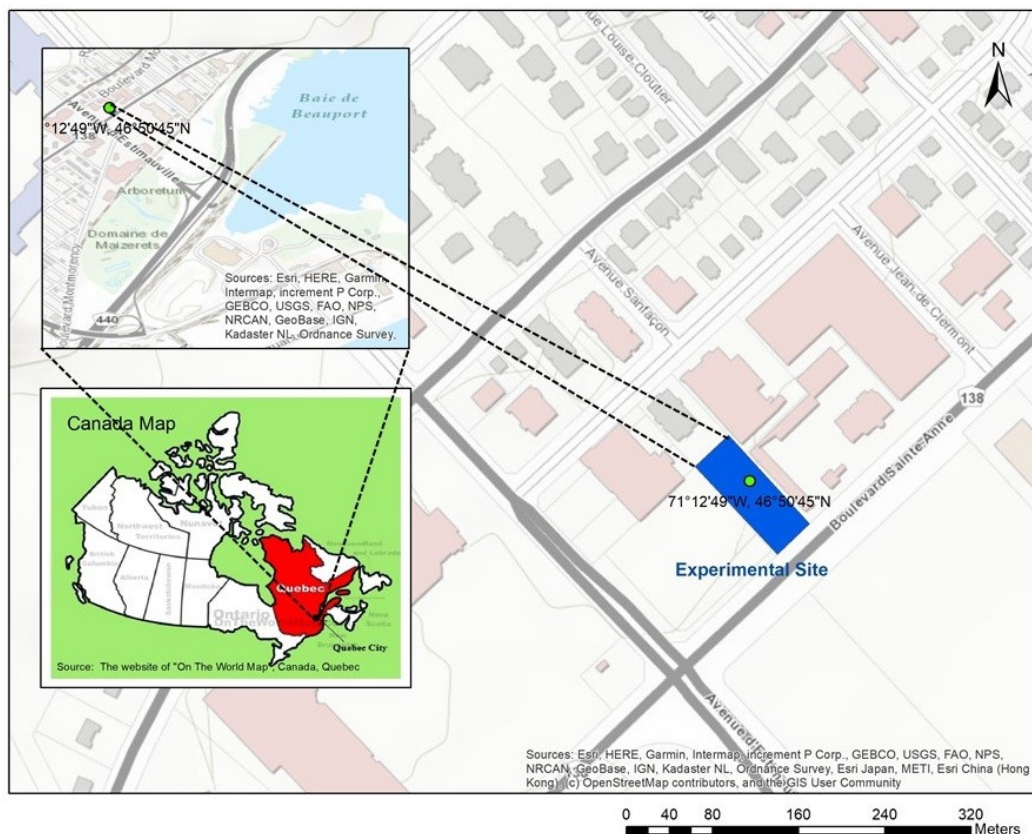

Figure 2 Map of the experimental site near the Baie de Beauport, northern shore of the St-Lawrence River, Quebec City, Canada.

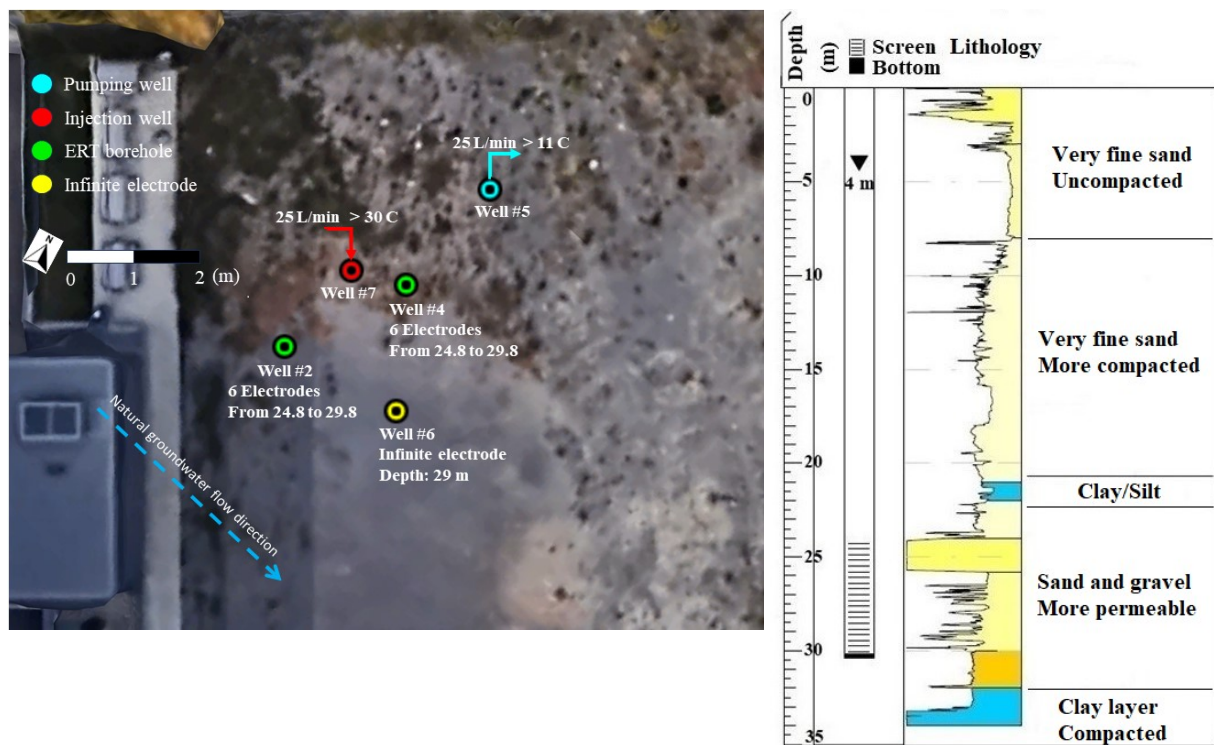(a)   (b)

Figure 3 a) Plan view and configuration of the pumping, injection and ERT monitoring wells. The blue dashed line shows the direction of natural groundwater flow. b) CPT lithological log in well 2 and scheme of the installed casing.

3.2 Hydrogeological framework

Five wells were installed to perform the heat-tracing experiment (Figures 3 & 4 and Table 1). A pumping well (Well #5) was drilled in the northern part of the site, to supply the water that was heated and reinjected in Well #7. The Well #5 is hydraulically upgradient from the injection well (Well #7) and both are spaced five meters apart. Three monitoring wells were used to perform cross-borehole ERT monitoring where Well #2 and Well #6 are located in the southern part of the site and Well #4 in the middle of the site. Well #2 and #4 were equipped with six downhole electrodes with one meter spacing across the screened interval (between 24.8 and 29.8 m from surface), while an electrode was mounted at the bottom of Well #6 (depth of 29 m) as an infinite electrode to perform pole-dipole array (Figure 3 & 4). All wells were screened in the aquifer between 24 m and 30 m from surface (Figure 3), except Well #4 that is totally screened (Table 1). The groundwater flow direction is west to east, which is almost perpendicular to the cross-section of Well #2 and Well #4.
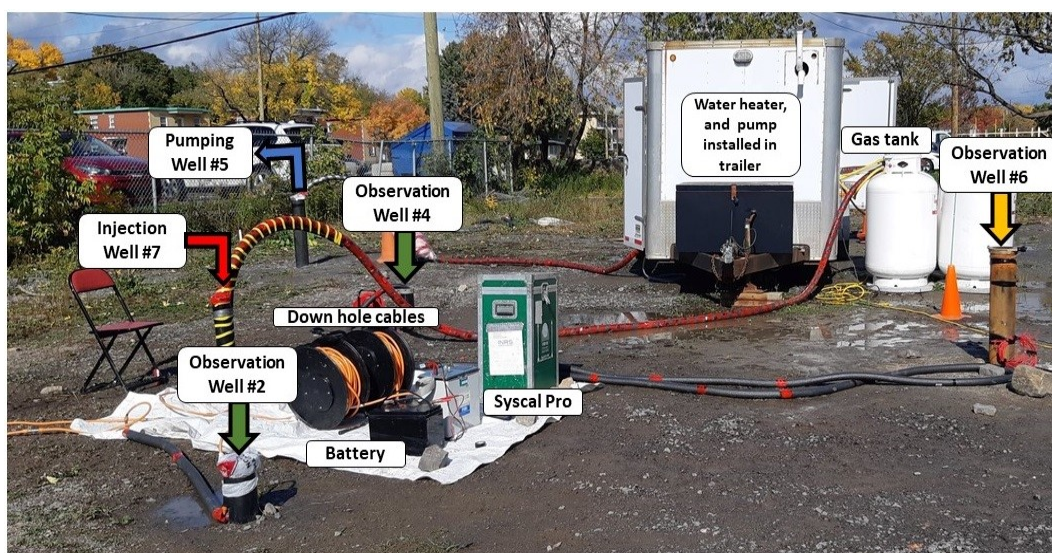
Figure 4 Heat-tracing equipment setup at the site, and location of pumping, injection, and observation wells. The position of pumping, injection and three ERT monitoring wells, downhole cable run into the bottom of well #2 and #4. Water heater was installed in trailer.

Table 1 The well characterization.

Well name	Final depth (m)	Screen depth (m)
Well #2	29.18	[23.18-29.18]
Well #4	30.95	[5.45-30.95]
Well #5	31.82	[25.82-31.82]
Well #6	31.98	[25.98-31.98]
Well #7	31.86	[25.86-31.86]

Temperature sensors and water level loggers were installed in the wells prior to the initiation of the heat injection experiment to measure the aquifer background temperature and hydraulic gradient respectively.

The thermal response test (TRT) was performed in Well #4 and Well #6 to calculate the thermal conductivity of the different lithostratigraphic units (Lee et al. 2021). An electrical heating cable with a power of 35.6 ($W.m^{-1}$) was installed into both wells and the duration of injection and recovery phase was 103.5 hours.

Table 2 The results of two TRT were performed in Well #4 and #6. The interpreted thermal conductivity in Well #6 is more reliable.

Well	Depth	Temperature sensor Spacing (m)	Number of temperature sensor	Thermal conductivity (Aquifer) $(W.m^{-1}.K^{-1})$	Thermal conductivity (Top of Aquifer) $(W.m^{-1}.K^{-1})$
Well #4	[5.95-30.95]	1	26	[55.89-427.23]	[1.49-14.7]
Well #6	[4.48-31.48]	1	25	[1.5-3.29]	[1.48-1.5]

The TRT result (Table 2) for Well #4 shows extreme values of thermal conductivity which were not expected for both aquifer and top of the aquifer (Poulin et al. 2013). Therefore, Well #6 results were used to specify thermal conductivity to different lithostratigraphic units. Figure 5 depicts the monitoring temperature data (blue points) at the depth of 28 m in Well #6 during injection (Fig. 5a) and recovery (Fig. 5b) respectively.
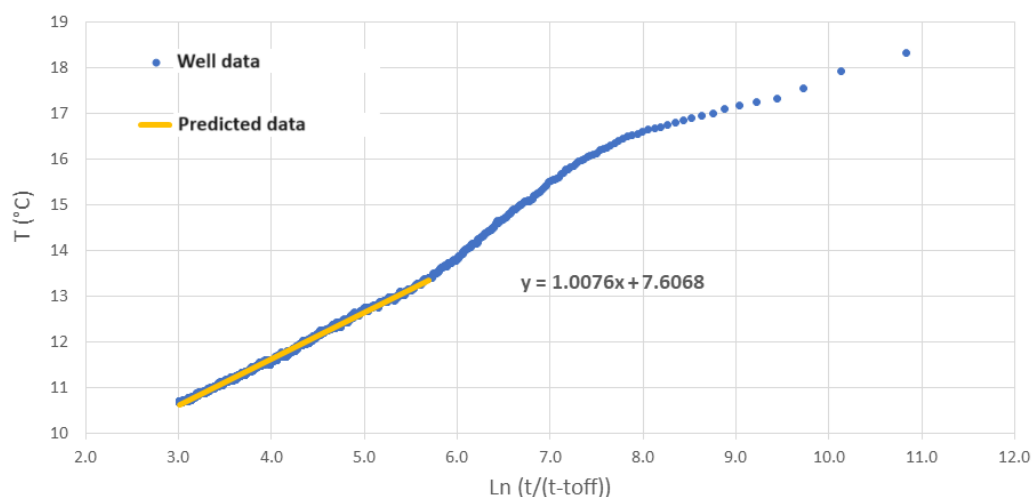
(a)
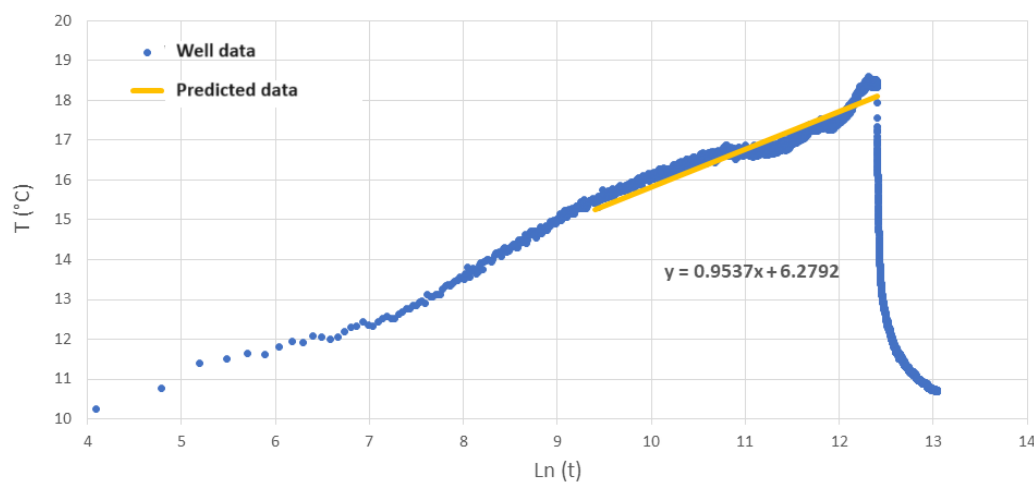
(b)

Figure 5 The TRT analysis plots. (a) Injection period (b) recovery period. The orange line is the fitted line to the recorded temperature data to estimate thermal conductivity.

The two thermal conductivity values were obtained based on the Infinite Linear Source (ILS) method. ILS is a well-known method for analyzing TRT data that enables us to calculate underground thermal conductivity and thermal resistance of the borehole (Raymond 2019; Focaccia et al. 2013). The orange line in Figure 5 shows the fitted line to the injection (Figure 5a) and the recovery temperature monitoring data (Figure 5b). The calculated thermal conductivities for the duration of injection and recovery are equal to 1.29 ($W.m^{-1}.K^{-1}$) and 1.22 ($W.m^{-1}.K^{-1}$) respectively. Since the recovery data are more uniform, the interpreted thermal conductivity using recovery period data is said more reliable.

Ten air-pressurized slug tests were also conducted in Well #2 (six tests) and Well #3 (four tests) to estimate hydraulic conductivity (Springer & Gelhar 1991). The slug test analysis estimates the aquifer hydraulic conductivity's range in Well #2 and Well #3 as [1.12-3.03]$\cdot10^{-4}$ ($m.s^{-1}$) and [2.29-2.89]$\cdot10^{-4}$ ($m.s^{-1}$) respectively.

The heat-tracing experiment started on September 1, 2020 and lasted for a period of 75 hours. The pumping and injection rates decreased over time from 25 to 5.7 ($l.min^{-1}$) (Table 3) due to reduction of Well #7 capacity over time cased by Biofouling. Indeed, inspection of Well #7 after the experiment showed important iron oxides precipitations within the well casing and screens. The pumped water went directly through a water heater and was reinjected into Well #7 at a temperature of approximately 30 ^{o}C (Table 3). The baseline groundwater temperature in the aquifer prior to the heat-tracing experiment was 10.3 ^{o}C.

Table 3 Pumping (negative values) and injection (positive values) rates time-series.

Start (min)	End(min)	Flow rate ($l.min^{-1}$)	Temperature (^{o}C)
0	1395	±25	30
1395	1793	±15.7	30

1793	2480	±10.6	30
2480	3016	± 5.7	30
3016	10080	0	

4. Results

4.1. Numerical model of groundwater flow and heat transfer

For numerical simulations we set the model size to be 14×19×14 m along North, West and depth respectively. We performed a preliminary test for studying the mesh resolution by running a few simulations with a different mesh size and verifying the stability of the solution. Finally, 3D triangular mesh containing 29 slices and 28 layers with a uniform thickness of 0.5 m was generated. Each slice and layer of the mesh is composed of 3,737 nodes and 7,335 elements, respectively with a minimum element size of 0.2 m. Therefore, the 3D mesh consists of 205,380 elements and 108,373 nodes.

The groundwater flow and heat transfer boundary conditions need to be defined to reproduce heat-tracing experiment accurately. Pumping and injection wells have been considered as multilayer well hence the flow is specified to each layer regarding to their hydraulic conductivity value. Type I (constant heads) hydraulic head boundary condition were imposed from the top to the bottom of the east and west edge of modeling mesh to reproduce a horizontal hydraulic gradient of (0.003 m.m^{-1}) representative of measured hydraulic conditions prior to the test (Diersch 2014). Type I (constant temperature) boundary condition was also imposed to the injection well and from top to the bottom of the east edge of the model to maintain water inflow temperature same as the baseline temperature. Baseline measured temperatures of 10.3 $^{\circ}$C were assigned to each node within the model domain to represent the initial subsurface conditions.

In this study, the hydraulic conductivity is the state variable to be updated by assimilation of cross-borehole ERT data. An initial ensemble of 100 realizations of 3D hydraulic conductivity field was generated using unconditional Sequential Gaussian Simulation (SGS) approach based on prior information from field measurements. The SGS simulation was carried using SGeMS (Remy et al. 2009), an open-source geostatistical simulation software. The slug test result, lithological log and bibliographic data (Hwang et al. 2017; Poulin et al. 2013) then supported the selection of the range of hydraulic conductivity values for each lithostratigraphic unit in the first stages of the data assimilation experiment which is reported in Table 4.

Table 4 Hydraulic conductivity values assigned to the lithostratigraphic units (Poulin et al.

2013; Hwang et al. 2017)

Layer	Depth (m)	Hydraulic conductivity (log10 K (m. s^{-1}))	
Very fine sand	[19-21]	Mean: -6	Standard Deviation = - 0.33

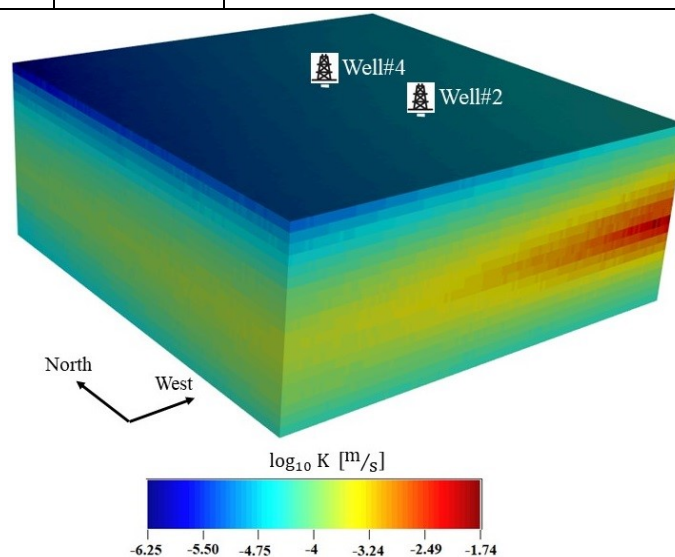| Clay/silt	[21-22]	Mean: -7	Standard Deviation = - 0.33
Sandy-gravel Aquifer	[22-32]	Mean: -4	Standard Deviation = - 0.5
Compacted clay	[32-33]	Mean: -9	Standard Deviation = - 0.33

Figure 6 One SGS realization of the 3D distribution of hydraulic conductivities (log$_{10}$ K [m/s]).

Lithological log and TRT test results were used to define the thickness and thermal conductivity of each layer respectively.

We developed a transient model of groundwater flow and heat transfer for a heat-tracing experiment using a finite element model. The numerical model is solving the differential equations using a finite element mesh and FEFLOW simulator (FEFLOW 7.3). The API functions of FEFLOW 7.3 (DHI, n.d.) were used to reassign updated K at each monitoring time-step and retrieve simulated groundwater temperatures under similar conditions as imposed through the heat-tracing experiment. As additional conditions, we applied the conduction-forced convection heat transfer mode to the model, The density of water was considered as a function of temperature and the heat injection experiment was performed in an unconfined sandy-gravel aquifer.

4.2 Time-lapse cross borehole ERT dataset

The Time-lapse Cross borehole ERT measurements were carried out in a cross-section of the Wells #2 and Well #4, which is perpendicular to the natural ground water flow direction. The electrode array configurations of Dipole-Dipole, Pole-Dipole and Pole-Tripole were acquired to conduct a monitoring cross-borehole ERT survey (Loke 2013). All possible combinations of electrodes were considered, except those with two current electrodes in the same well, as they cause a short-circuit between the current electrodes. Finally, the measuring

sequence consists of 596 pairs of normal and reciprocal quadrupoles that took approximately 30 minutes to measure. Due to the presence of clay layers overlying and underlying the sandy-gravel aquifer (Figure 3b), the ERT measuring time was set up to 500 milli-seconds to reduce the induced polarization (IP) effects on direct current (DC) measurements.

A total of 11 cross-borehole ERT surveys were conducted during a period of 7 consecutive days. All data set has been filtered in terms of outliers and reciprocal errors (Binley et al. 1995) before calculating the mean apparent electrical resistivity. The mean apparent electrical resistivity for the background data set was 42.55 (ohm.m). As expected, the apparent resistivity decreased during the heated water injection phase by 9% and started increasing during the recovery phase after the end of heat injection (Figure 7).
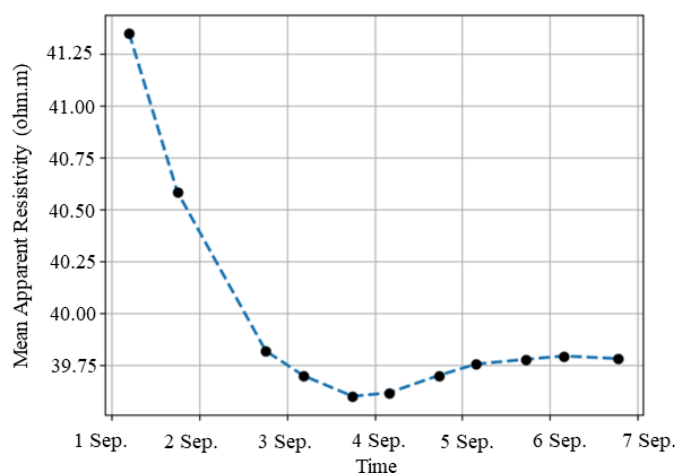

Figure 7 The mean apparent electrical resistivity (ohm.m) of each monitoring time-step versus the elapsed time since the beginning of the heat-tracing experiment. Minimum mean apparent electrical resistivity was measured after 3.75 days and then started increasing slightly.

The measurement error estimation is crucial for data assimilation approach as the accuracy of results is subject to that parameter (Evensen 2009). The measurement is used to calculate measurement perturbation matrix and measurement error covariance matrix. The reciprocal measurement error model was considered to provide the measurement error model for EnKF (Binley et al. 1995). For all ERT monitoring time steps, each pair of normal and reciprocal measurements were used to calculate the reciprocal errors and a reference line is fitted to the top of the data (Figure 8):
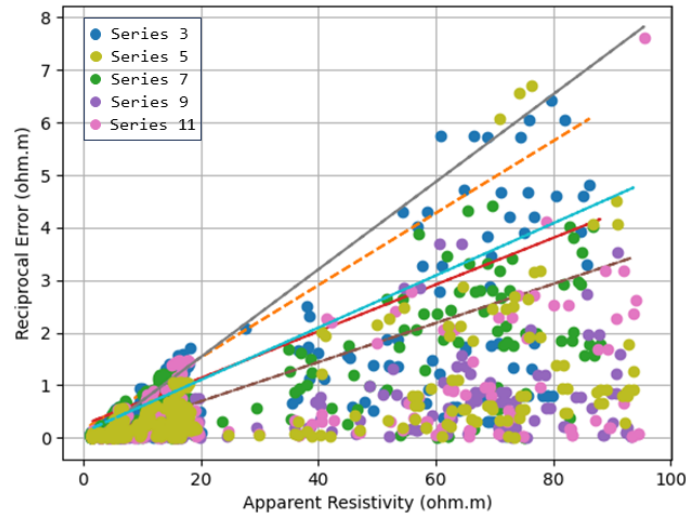
Figure 8 Reciprocal measurement errors as a function of apparent resistivity for five datasets from cross-borehole ERT surveys. The solid/dash lines show the fitted reference line to the top of each dataset.

$$\mathbf{Err}^m = a * \boldsymbol{\rho}_a + b \tag{11}$$

where $\mathbf{Err}^m$ is the measurement error in ohm.m, $\boldsymbol{\rho}_a$ is the measured apparent resistivity (ohm.m), a and b are slop and intercept of fitted reference line respectively.

Equation 11 was used to predict the measurement error for each normal quadrupole in cross-borehole ERT array. Consequently, an error distribution is provided for each ERT monitoring time step, allowing for the generation of random errors to perturb the measurements (Equation 7) and create observation error covariance matrix (Equation 10), needed in the presented approach.

4.2 ERT data assimilation and prediction

The results of time-lapse inversion of ERT data were earlier presented by Shariatinik et al. (2021) and Shariatinik (2022). The cross-borehole ERT data time lapse inversions demonstrated that ERT models can be used for estimating the three-dimensional spatial extent of a heat plume in combination with groundwater temperature data in wells (Shariatinik et al. 2021). Hence, being able to replicate cross-borehole ERT data at each monitoring time step was considered an important criterion for the success of the cross-borehole ERT data assimilation experiment.

In this work, the ERT data were divided into assimilation and prediction datasets, where the first nine time-steps were used for data assimilation, while the last two were used to predict the future state of the system. In more details, firstly, the ERT data were assimilated to update the ensemble of K; while in the second step, we skip the ERT data

assimilation step of flowchart (Figure 1) to see if the numerical model of groundwater flow and heat transfer (using updated ensemble of K) is able to predict the future state of the ground water temperature accurately.

The results are plotted in Figure 9, where we show the mean measured and forecasted apparent resistivity plots over the 11 time-steps for different ensemble size. A comparison of the three plots in Figure 9 clearly shows the effect of the ensemble size on the rate of convergence of the forecasted apparent resistivity values to the observed ones.

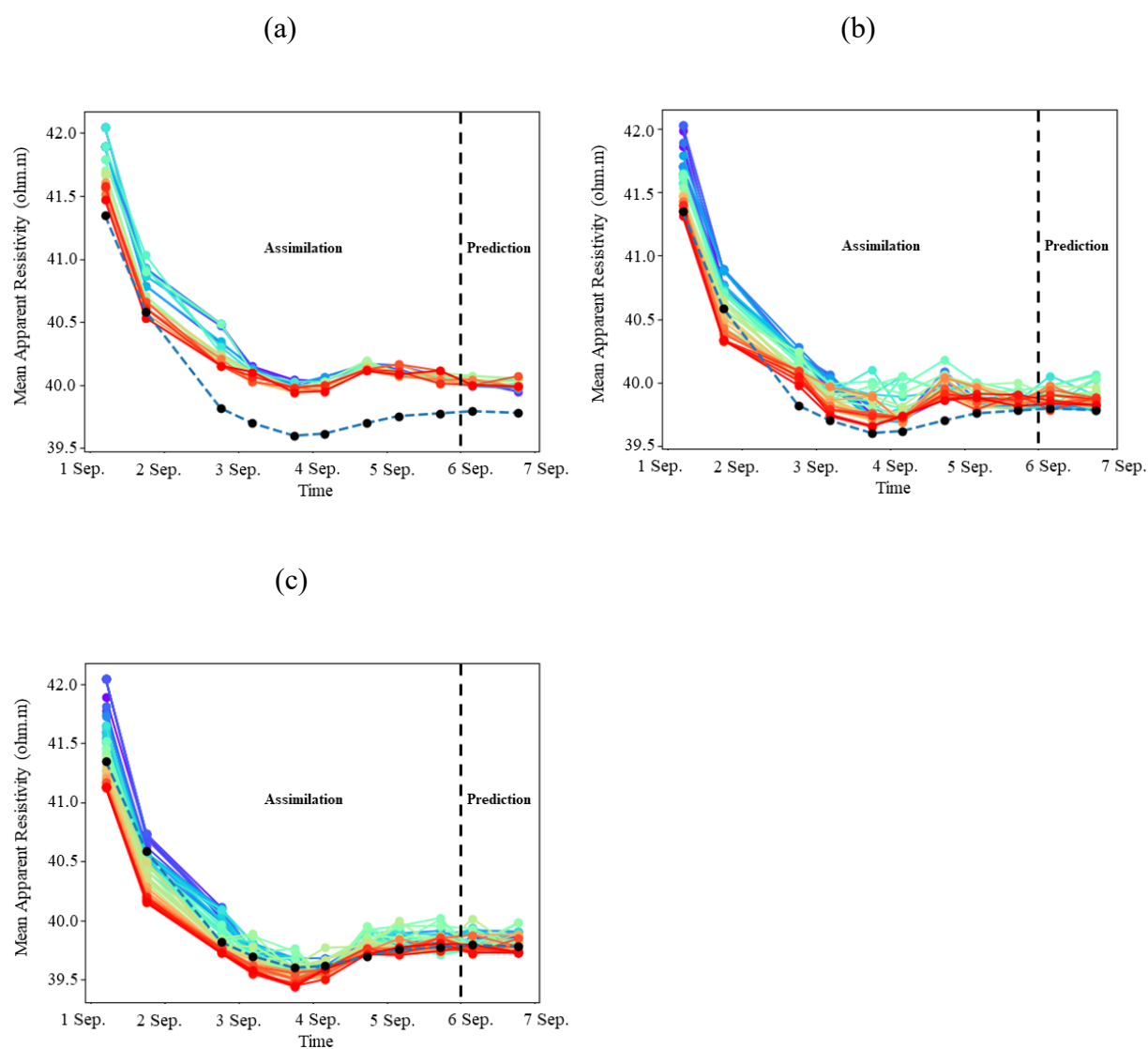(a)   (b)

(c)

Figure 9 Mean apparent resistivity versus time for the 11 time steps of the heat-tracing experiment. The observed data are marked with dashed line and black point, while colored curves and points indicate forecasted data for ensemble size of 20 (a), 40 (b) and 60 (c) respectively.

Using 20 realizations (Figure 9a), the EnKF was not able to converge to an unbiased estimation and the standard deviation of simulated apparent resistivity decreased dramatically, from 0.62 ohm.m to 0.2 ohm.m up to the ninth time step (end of data assimilation) and the predicted apparent resistivity were overestimated. To handle these shortcomings, the ensemble size was increased to 40 realizations (Figure 9b) which improved the match between forecasted apparent resistivity with measured apparent resistivity even though the ensemble variance is still high (0.44).

The solution with an ensemble of 60 realizations, gives a good match between forecasted and observed apparent resistivity values with a reasonable computational cost.

On the other hand, the simulated groundwater temperatures for sixty realizations were compared to the measured temperature from a temperature sensor located at a depth of 28 m at Well #4. Figure 10 shows the simulated groundwater temperatures compared to measured temperature during the injection and recovery period. Except for the first two monitoring steps the simulated temperatures converge to the actual measurement that can be due to this fact that hydrogeological model is in the early steps of assimilation and is not still calibrated.
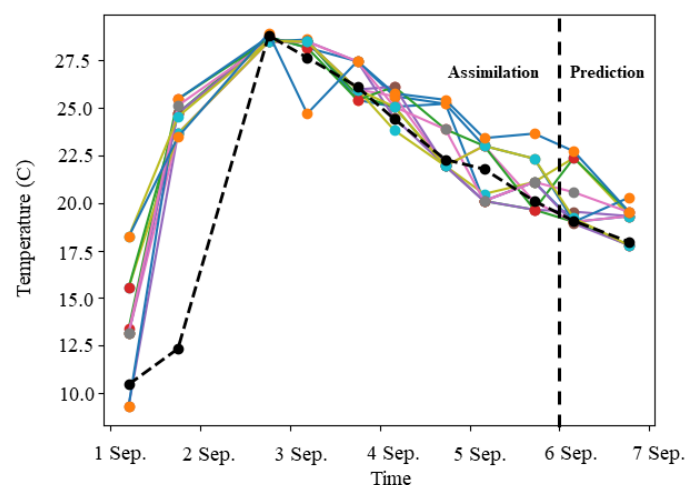

Figure 10 Temperature versus time for the 11 time steps of the heat-tracing experiment. The measured temperature at the depth 28 m of well#4 is marked with dashed line while the colored solid line represents the modeled temperatures at the same depth.

The prior and posterior distribution (Equation 7) of K ensemble of size 60 is presented in Figure 11. In addition, the mean and standard deviation (std) of K distribution, prior and post assimilation experiment is reported to give an idea about K distribution change due to cross-borehole ERT data assimilation. The standard deviation value of K decreased through the assimilation experiment, but it did not collapse. After nine steps of cross-borehole ERT data assimilation, the mean value of K converged to the geometric mean of slug tests results (Poulin et al. 2013), although the initial K distribution is negatively biased compared to direct measurement with slug tests.
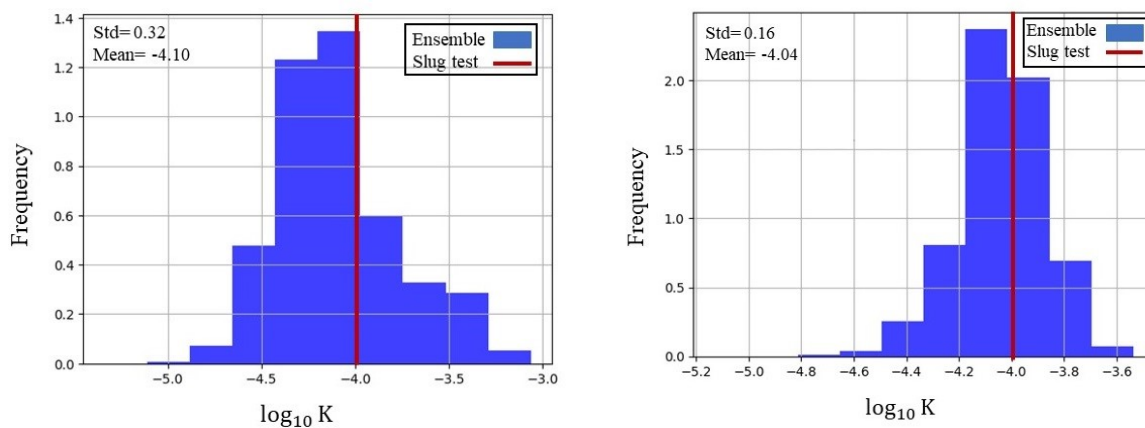
Figure 11 (a) Initial K distribution of ensemble before the beginning of the assimilation experiment. (b) posterior K ensemble distribution after nine assimilation steps. The vertical red line marks the geometric mean of slug tests result.

Figures 12a and 12b show the mean of the prior and posterior ensemble of K in the cross-sectional area of Well #2 and Well #4 respectively. where the range of K values in Figure 12b are higher than range of K in Figure 12a. This is consistent with the results in Figure 11 where the mean of distribution of posterior ensemble of K moved toward higher K values after nine assimilation steps. It should be noted that the same K distribution is used by SGS across whole aquifer thickness to generate prior ensemble of K (Figure 12a, Figure 6). A zone with higher range of K in Figure 12b from depth of 27 m to the bottom of aquifer was created after nine steps of cross-borehole ERT data assimilation. The lithological log (Figure 3b) shows the same layer at the bottom of aquifer with a higher quantity of gravel associated with higher K. The absolute difference between prior and posterior K ensemble was calculated in order to highlight the magnitude improvement of K in every pixel of the cross-sectional area (Figure 12c). The standard deviation values of posterior K ensemble plotted in Figure 12d shows lower values in the interval depth of 25 m to 30 m of cross-section where the downhole electrodes were mounted, demonstrating that the rate of convergence to an unbiased K estimation is higher for the area which has been covered by cross-borehole ERT data.
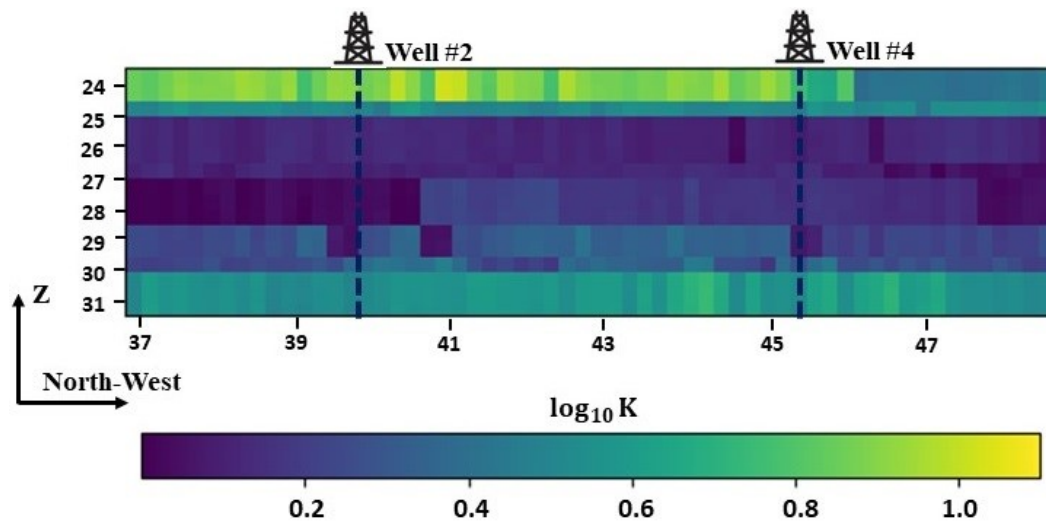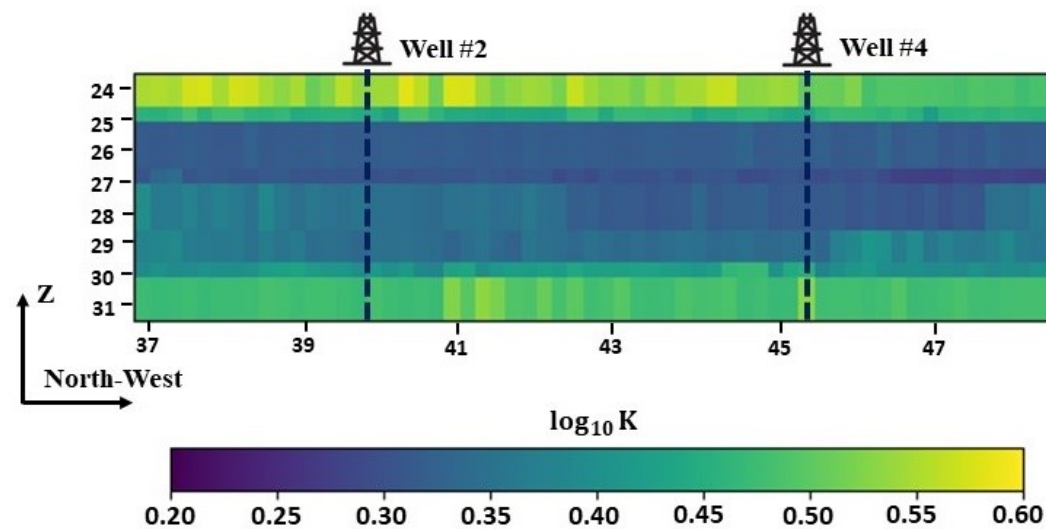
(a)
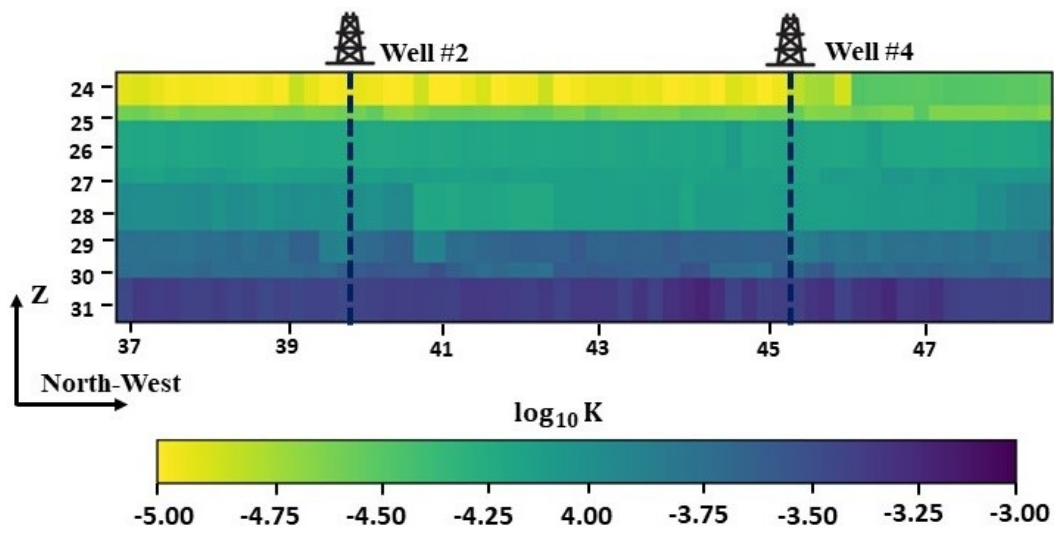
(b)
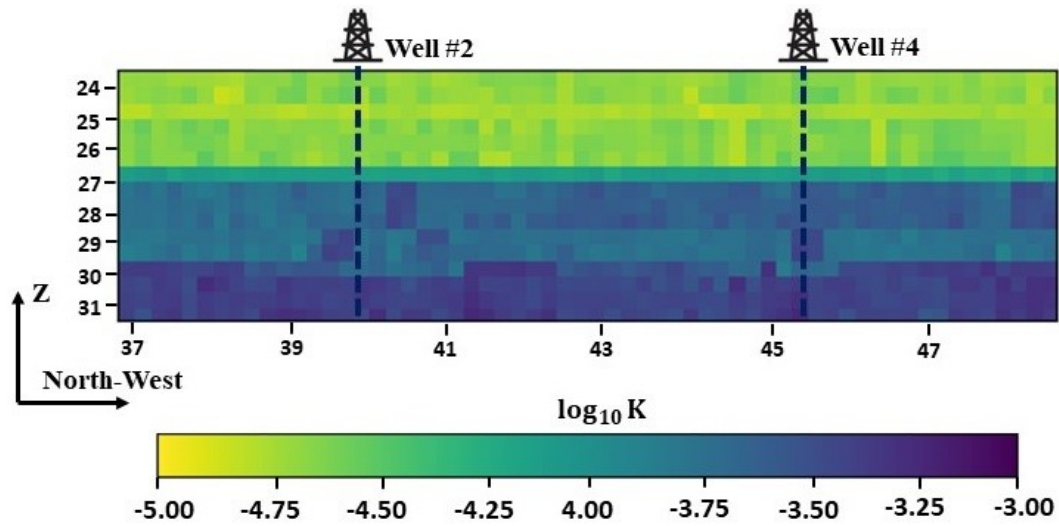
(c)

(d)

Figure 12 Hydraulic conductivity cross-section between Well #2 and Well #4. (a) Initial K distribution. (b) K distribution after last assimilation step. (c) Absolute difference between cross-sections of Figure 12a and 12b which shows the updated values during assimilation experiment. (d) Standard deviation of posterior K distribution at each pixel of cross-section. Each pixel size is 0.5 m by 0.2 m along Z and X axis respectively.

5. Discussion and conclusions

ERT observations are indirect and low-cost measurements in Earth's shallow subsurface. They are worthwhile to be considered for data assimilation experiment as they provide high spatial and temporal resolution data. In this paper, we investigated the implementation of the time-lapse cross borehole ERT data assimilation during a heat-tracing

experiment that allows to reproduce the hydraulic conductivity heterogeneity of a shallow sandy-gravel aquifer. The study provides a numerical tool for eventually simulating the operation of a GWHP system. To the best of our knowledge, this is the first time that ERT data assimilation using EnKF has been applied in the scope of a heat tracing experiment to assess the GWHP potential.

In this context, the process is carried out in two steps of assimilation and prediction. The first step consisting of nine ERT datasets where ERT data are assimilated to update the hydrogeological model. In the second step, the last two ERT datasets are masked to assess the reliability of the updated hydraulic conductivity model to predict the future state of the system. The comparison between modeled electrical resistivity values and field measurement in both steps shows a good agreement, confirming to the reliability of the approach. The assimilation experiment was repeated to optimize the ensemble size. Finally, the ensemble size of sixty was chosen since the modeled ERT measurement converges to field measurements, the ensemble variance reduction due to spurious correlation (Evensen 2009) was acceptable in comparison with ensemble size of 20 and 40 and run time was reasonable. To further test the approach, the coupled temperature model was also compared with the measured temperature at the sensor location which show a good agreement while temperature was an independent variable during the assimilation process and hydrogeological model was not updated with respect to the observed temperature values.

The proposed workflow integrates different methods and numerical models including ground water flow and heat transfer modelling, electrical forward modeling, petrophysical relationship and data assimilation using EnKF. A series of Python codes were used to combine and exchange information between components of the workflow (Shariatinik 2022).

We demonstrated that the assimilation of cross-borehole ERT data into numerical model of groundwater flow and heat transfer through a heat tracing experiment is an effective tool to characterize the aquifer hydraulic conductivity heterogeneity, which is essential in the process of designing a GWHP system as the process of sizing GWHP system is mainly based on the result of the numerical model before the installation of the GWHP system (Raymond 2019). In this regard, the definition of K heterogeneity has a significant effect on the accuracy of numerical modelling results.

In addition, this method can be considered as a powerful approach to evaluate subsurface properties uncertainty, as it provides a range of values for desired variable using ensemble of realizations. The comparison between prior and posterior distribution of hydraulic conductivity with field slug test results confirm that the proposed approach can make the distribution move toward the mean of slug test results. Moreover, the simulated groundwater temperatures show a reasonable match with measured ground water temperature after the third data assimilation step. Therefore, the possibility of using EnKF to predict the future state of a geothermal system such as heat storage systems or deep geothermal resources in the long term could be attractive in further studies.

References

Aghasi, A., Mendoza-Sanchez, I., Miller, E.,; Ramsburg, C. A., Abriola, L. M., (2013) A geometric approach to joint inversion with applications to contaminant source zone characterization. *Inverse Problems,* Volume 29, p. 11514.

Anderson, M. P., (2005) Heat as a Ground Water Tracer. *Ground Water ,* 43(6), pp. 951-968.

Archie, G. E., (1942) The Electrical Resistivity Log as an Aid in Determining Some Reservoir Characteristics. *Transactions of the AIME,* 146(01), pp. 54-62.

Blanchy, G., Saneiyan, S., Boyd, J., McLachlan, P., & Binley, A., (2020) ResIPy, an Intuitive Open Source Software for Complex Geoelectrical Inversion/Modeling. Computers & Geosciences, February, 104423. https://doi.org/10.1016/j.cageo.2020.104423.

Bayer, P., Attard, G., Blum, P. & Menberg, K., (2019) The geothermal potential of cities. *Renewable & Sustainable Energy Reviews,* Volume 106, pp. 17-30.

Binley, A., Ramirez, A. & Daily, W. D., (1995) *Regularised Image Reconstruction of Noisy Electrical Resistance Tomography Data.* Bergen, s.n., pp. 401-410.

Binley, A., S. Hubbard, S., A. Huisman, J., Revil, A., A Robinson, D., Singha, K., Slater, L. D., (2015) The emergence of hydrogeophysics for improved understanding of subsurface processes over multiple scales. *Water Resources Research,* 51(6), pp. 3837-3866.

Bouzaglou, V., Crestani, E., Salandin, P., Gloaguen, E., Camporese, M., (2018) Ensemble Kalman Filter Assimilation of ERT Data for Numerical Modeling of Seawater Intrusion in a Laboratory Experiment. *Water,* 10(4).

Camporese, M., Cassiani, G., Deiana, R. & Salandin, P., (2008) Assessment of local hydraulic properties from Electrical Resistivity Tomography monitoring of tracer test experiments. *Water Resources Research,* 47(12).

Cultrera, M., Boaga, J., Di Sipio, E., Dalla Santa, G., De Seta, M., Galgaro, Antonio., (2018) Modelling an induced thermal plume with data from electrical resistivity tomography and distributed temperature sensing: a case study in northeast Italy. *Hydrogeology Journal,* 26(3), pp. 837-851.

Day-Lewis, F., Singha, K. & Binley, A., (2005) Applying petrophysical models to radar travel time and electrical resistivity tomograms: Resolution-dependent limitations. *Journal of Geophysical Research Atmospheres,* 110(B8).

DHI, M. P. b., n.d. *FEFLOW 7.3 Documentation.* [Online] Available at: feflow.info/html/help73/feflow/01_Introduction/morehelp/documentation.html

Diersch, H.-J. G., (2014) *FEFLOW, Finite Element Modeling of Flow, Mass and Heat Transport in Porous and Fractured Media.* New York: Springer.

Evensen, G., (1994) Sequential data assimilation with a nonlinear quasi-geostrophic model using Monte Carlo methods to forecast error statistics. *JOURNAL OF GEOPHYSICAL RESEARCH,* 99(C5), pp. 10143-10162.

Evensen, G., (2009) *Data Assimilation, The Ensemble Kalman Filter.* New York: Springer.

Focaccia, S., Tinti, F. & Bruno, R., (2013) A software tool for geostatistical analysis of thermal response. *Computers & Geosciences,* Volume 59, pp. 163-170.

Hayley, K., Bentley, L., Gharibi, M. & Nightingale, M., (2007) Low temperature dependence of electrical resistivity: Implications for near surface geophysical monitoring. *Geophysical Research Letters,* 34(18).

Hermans, T., Vandenbohede, A., Lebbe, L. & Nguyen, F., (2012) A shallow geothermal experiment in a sandy aquifer monitored using electric resistivity tomography. *GEOPHYSICS,* 77(1), pp. B11-B21.

Hermans, T., Wildemeersch, S., Jamin, P., Orban, P., Brouyère, S., Dassargues, A., Nguyen, Frédéric., (2015) Quantitative temperature monitoring of a heat tracing experiment using cross-borehole ERT. *Geothermics,* Volume 53, pp. 14-26.

Hwang, H.-T., Jeen, S.-W., Suleiman, A. A. & Lee, K.-K., (2017) Comparison of Saturated Hydraulic ConductivityEstimated by Three Different Methods. *Water,* 9(12).

Kaviany, M., (1995) *Principles of Heat Transfer in Porous Media.* New York, United States : Springer Press..

Lamarche, L., (2011) *Palaeoenvironmental evolution of quaternary dynamics in the Quebec City region: Application in three-dimensional and hydrogeological modelling. PhD thesis,* Quebec City: Institut national de la recherche scientifique-Centre Eau Terre Environnement.

Lee, V., Raymond, J., Rivard, C., Comeau, F. A., Newson, J., (2021) *Groundwater Heat Pump (GWHP) Systems to Fight Urban Heat Islands: Asolution for Canada's Major Cities.* Toronto, ON, Canada, s.n.

Loke, M., (2013) Tutorial: 2-D and 3-D electrical imaging surveys. *Geotomo software Malaysia.*

Maslin, M., (2004) *GLOBAL WARMING, A Very Short Introduction.* New York: Oxford University Press Inc..

Menke, W., (1984) *Geophysical Data Analysis: Discrete Inverse Theory.* NewYork: Academic.

Nima Raanes, P., (2016) PhD Thesis. Improvements to ensemble methods for data assimilation in the geosciences. *University of Oxford.*

Pidlisecky, A., Singha, K. & Day-Lewis, F. D., (2011) A distribution-based parametrization for improved tomographic imaging of solute plumes. *Geophysical Journal International,* 187(1), pp. 214-224.

Poulin, M. C. T., Comeau, G., Tremblay, Y., Therrien, R., Lemieux, J. M., Molson, J., Fortier, R., Therrien, P., Lamarche, L., Donati-Daoust, F., Bérubé, S., Nadeau, M. M., (2013) *Projet d'acquisition de connaissances sur les eaux souterraines du territoire de la Communauté métropolitaine de Québec (PACES-CMQ), Rapport final,* ville de Québec: Département de géologie et de génie géologique, Université Laval.

Raymond, J., (2018) Colloquium 2016: Assessment of subsurface thermal conductivity for geothermal applications. *Canadian Geotechnical Journal.*

Raymond, J., (2019) *Heat transfer applied to earth science- Course Note.* Quebec City, Canada, s.n.

Remy, N., Boucher, A. & Wu, J., (2009) *Applied Geostatistics with SGeMS, A User's Guide.* United Kingdom: Cambridge University Press.

Saar, M., (2011) Review: Geothermal heat as a tracer of large-scale groundwater flow and as a means to determine permeability fields. *Hydrogeology Journal,* Volume 19, pp. 31-52.

Saneiyan, S., Boyd, J., Blanchy, G. & McLachlan, P., (2018) *ResIPy documentation master file.* [Online] Available at: https://hkex.gitlab.io/resipy/

Shariatinik, B., Bouchedda, A., Gloaguen, E., Raymond, J., Fabien-Ouellet, G., (2021) A heat tracing experiment using cross-borehole time-lapse ERT. NSG2021 27th European Meeting of Environmental and Engineering Geophysics, Aug 2021. Volume 2021, pp. 1-5. https://doi.org/10.3997/2214-4609.202120041

Shariatinik, B., (2022) *Benyamin-Shariatinik.* [Online] Available at: https://github.com/Benyamin-Shariatinik/EnKF-ERT [Accessed 09 08 2022].

Singha, K. & M. Gorelick, S., (2006) Effects of spatially variable resolution on field-scale estimates of tracer concentration from electrical inversions using Archie's law. *GEOPHYSICS,* 71(3).

Springer, R. K. & Gelhar, L. W., (1991) *Characterization of large-scale aquifer heterogeneity in glacial outwash by analysis of slug tests with oscillatory response, Cape Cod, Massachusetts,* Reston: U.S. Geol. Surv. Water Res. Invest..

Tso, C.-H.M. et al., (2020) Integrated hydrogeophysical modelling and data assimilation for geoelectrical leak detection. *Journal of Contaminant Hydrology,* Volume 234.

Wikle, C. K. & Berliner, L. M., (2007) A Bayesian tutorial for data assimilation. *Physica D: Nonlinear Phenomena,* 230(1-2), pp. 1-16.

Xu, Y.S., Wang, X.-W., Shen, S.-L. & Zhou, A., (2020) Distribution characteristics and utilization of shallow geothermal energy. *Energy & Buildings,* Volume 229.

Yan, C. & Dongxiao, Z., (2006) Data assimilation for transient flow in geologic formations via ensemble Kalman filter. *Advances in Water Resources,* 29(8), pp. 1107-1122.